Electron momentum spectroscopy of xenon: A detailed analysis

J. P. D. Cook, I. E. McCarthy, J. Mitroy, and E. Weigold
Institute for Atomic Studies, The Flinders University of South Australia, Bedford Park, South Australia 5042, Australia
(Received 22 July 1985)

Accurate measurements of the 1000-eV noncoplanar symmetric $(e,2e)$ reaction on xenon are reported. Cross-section calculations are carried out with the use of both the plane-wave and distorted-wave impulse approximations. The distorted-wave impulse approximation accurately describes both the $5p^{-1}$ and $5s^{-1}$ angular correlations and their relative cross sections. It also describes accurately the $5p_{3/2}^{-1}$:$5p_{1/2}^{-1}$ branching ratios if Dirac-Fock target wave functions are used. The branching ratios show the inadequacy of Hartree-Fock wave functions for xenon. The plane-wave impulse approximation overestimates the $5s^{-1}$ cross section relative to the $5p^{-1}$ and underestimates the cross section at large angles. The $5s^{-1}$ spectroscopic factors are assigned up to a separation energy of 45 eV, and the distorted-wave impulse-approximation calculation verifies that all the $5s^{-1}$ strength has been found. The spectroscopic factors for the $5s^{-1}$ manifold are obtained at 1000 and 1200 eV at a number of angles and are found to be independent of incident energy and ion recoil momentum. The spectroscopic factor for the lowest $5s^{-1}$ transition at 23.4 eV is 0.37 ± 0.01, whereas that for the ground-state $5p^{-1}$ transition is greater than or equal to 0.98.

I. INTRODUCTION

The noncoplanar symmetric $(e,2e)$ reaction is the basis of electron momentum spectroscopy (EMS).[1] It is a kinematically complete ionization measurement carried out on gas atoms or molecules under conditions of maximum momentum transfer to the knocked-out electron. These conditions are equal final-state electron energies ($E_A=E_B=E_F$), which are held fixed over the course of the experiment, and equal polar angles $\theta\approx45°$ for the final-state electron momenta. The energy states ϵ_s of the ion are scanned by varying the incident energy E_0. The profile of recoil momentum p is scanned for each ion state from approximately zero to several atomic units by varying the relative azimuthal angle ϕ of the final-state momenta.

At high enough total energy the momentum profile is given to a good approximation by the spherically averaged square modulus of the characteristic momentum-space orbital of the knocked-out electron. This is the orbital for which the leading configuration in a configuration-interaction expansion of the ion is a hole coupled to the target Hartree-Fock ground state. It characterizes the symmetry manifold of the ion state. This approximation, the plane-wave impulse approximation (PWIA), is valid up to some maximum momentum $p_{\max}$, which at the energies normally used ($\gtrsim$1000 eV) is at least 1 a.u. The criterion for sufficiently high energy is purely experimental. The structure information derived from the experiment must be independent of the total energy.

Inner-valence states of atoms and molecules usually consist of fragments of an orbital split by final-state configuration interaction. The characteristic orbital of each fragment is identified by its momentum profile. If all the fragments of a particular orbital are found in an experiment, the summed crossed section for them is equal to the cross section for the orbital, in the approximation that the Hartree-Fock configuration dominates the target ground state. The relative cross sections for the fragments, normalized to a sum of unity, are the spectroscopic factors or pole strengths. This interpretation is checked by the total-energy independence of the spectroscopic factors and the relative momentum profiles for different summed orbitals.

In the case of small molecules[1] these checks have always been obeyed when the momentum profiles are calculating using the PWIA. For inert-gas atoms spectroscopic factors for inner valence ^2S states have always been determined consistently at $p\sim0$, independent of total energy, by relative cross sections within the corresponding symmetry manifold. However, the ultimate confirmation, the comparison of momentum profiles between orbitals, has required the distorted-wave impulse approximation (DWIA).[1] Relative momentum profiles have been correctly calculated for the valence s and p manifolds of neon[2] and argon,[3] the latter to an accuracy of 3%. Momentum-profile shapes are correctly described for all measured momenta by the DWIA for these targets and for helium[4] and xenon[2]. However, relative s and p profiles were not correct for the previous xenon analysis.[2]

The present work describes more accurate experiments on xenon at $E=1000$ eV and $\theta=45°\pm0.1°$ and $E=1200$ eV and $\theta=45.7°\pm0.2°$. The $5p^{-1}$ and $5s^{-1}$ angular correlations obtained at 1000 eV are analyzed using the DWIA and relativistic orbitals. Details of the analysis of $(e,2e)$ experiments using the DWIA are given in Ref. 3. Although a relativistic description of the target wave function is necessary for a high-Z system, when the continuum electron energies are small (in terms of the electron rest mass), the relativistic form of the impulse approximation reduces to the nonrelativistic form.[5] Therefore, in the present analysis the nonrelativistic forms of

the impulse approximation have been used in conjunction with the relativistic form of the atomic wave function.

It has been known for some time that the dominant $5p^{-1}$ transition leading to the ion ground-state doublet has a spectroscopic factor close to unity, whereas the $5s^{-1}$ manifold is severely split.[1,6] We report here accurate measurements of both the $5p^{-1}$ and $5s^{-1}$ spectroscopic factors. The $5s^{-1}$ spectroscopic factors are obtained as a function of momentum p at both 1200 and 1000 eV total energies.

In order to identify the causes of the complex structure associated with the $5s^{-1}$ manifold, we have carried out relativistic configuration-interaction calculations of the target ground-state and residual ion states. The calculations were also undertaken in order to determine whether initial- and final-state configuration interactions have any influence on the $5p_{3/2}^{-1}$ and $5p_{1/2}^{-1}$ cross-section ratios. Values for these ratios had previously been measured[7] as a function of recoil momentum at 1200 eV total energy. The ratios were in agreement with predictions using Dirac-Fock wave functions and disagreed with Hartree-Fock (i.e., nonrelativistic) wave functions. We report further measurements at 1000 eV and use them to differentiate between the plane-wave and distorted-wave results.

II. GENERAL THEORY OF THE $(e,2e)$ REACTION

The plane-wave impulse approximation for the $(e,2e)$ reaction has previously[1] been written in terms of a general notation for the many-body wave functions of the target and ion. Here we give it in a more explicit notation[8] applicable to structure calculations. We explain the relationship of the general case to the target Hartree-Fock approximation, which gives a valid and practical simplification in many cases of interest.

The differential cross section in terms of the electron momenta $\mathbf{k}_0,\mathbf{k}_A,\mathbf{k}_B$ (in obvious notation) is

$$\frac{d^5\sigma}{d\hat{\mathbf{k}}_A d\hat{\mathbf{k}}_B dE_B}=(2\pi)^4\frac{k_A k_B}{k_0}f_{ee}G_f(p)\ , \tag{1}$$

where the electron-electron collision factor f_{ee} is the square modulus of the appropriate half-shell Mott-scattering t-matrix element averaged over electron-spin degeneracies,

$$f_{ee}=\frac{1}{(2\pi^2)^2}\frac{2\pi\nu}{\exp(2\pi\nu)-1}\left\{\frac{1}{|\mathbf{k}_0-\mathbf{k}_A|^4}+\frac{1}{|\mathbf{k}_0-\mathbf{k}_B|^4}-\frac{1}{|\mathbf{k}_0-\mathbf{k}_A|^2}\frac{1}{|\mathbf{k}_0-\mathbf{k}_B|^2}\cos\left[\nu\ln\left[\frac{|\mathbf{k}_0-\mathbf{k}_B|^2}{|\mathbf{k}_0-\mathbf{k}_A|^2}\right]\right]\right\}, \tag{2}$$

$$\nu=1/|\mathbf{k}_A-\mathbf{k}_B|\ ,\quad \mathbf{p}=\mathbf{k}_A+\mathbf{k}_B-\mathbf{k}_0\ . \tag{3}$$

The structure factor $G_f(p)$, written in terms of magnetically degenerate initial and final states, is

$$G_f(p)=\sum_{M_0,M_f}|\langle \mathbf{p}\Psi_f{:}J_fM_f\,|\,\Psi_0{:}J_0M_0\rangle|^2/(2J_0+1)\ . \tag{4}$$

For an atomic target with total-angular-momentum quantum number J_0 the magnetically degenerate target eigenstates $|\Psi_0{:}J_0M_0\rangle$ constitute a basis for a representation of the point group SU(2) of the target which has rank J_0 and dimension $2J_0+1$. The vector index of the representation space is M_0 (magnetic quantum number).

The matrix element in (4) is the probability amplitude that Ψ_f is obtained by annihilating an electron of momentum $\mathbf{p}$ and spin coordinate σ in the target state Ψ_0. We use second-quantized notation, in which the operator that annihilates such an electron is

$$\sum_{j,\alpha,m}\phi^j_{\alpha m}(\mathbf{p},\sigma)a^j_{\alpha m}\ . \tag{5}$$

The function $\phi^j_{\alpha m}$ is the single-particle orbital in momentum-spin space for total angular momentum j with projection m. In a many-body calculation the effect of certain complete manifolds of orbitals is often represented by replacing the manifolds with pseudostates (usually denoted by the use of a bar, e.g., $\bar{6s}$). The notation $\phi^j_{\alpha m}$ includes pseudostates. The quantum number j and the label α together uniquely specify the orbital, apart from the projection number m. The operator $a^j_{\alpha m}$ is the usual fermion annihilation operator with quantum labels j, α, and m. The orbital $\phi^j_{\alpha m}(\mathbf{p},\sigma)$ is defined by

$$\phi^j_{\alpha m}(\mathbf{p},\sigma)=\phi^j_\alpha(p)y^{jl}_m(\hat{\mathbf{p}},\sigma)\ , \tag{6}$$

where y^{jl}_m is a normalized spin-angle harmonic

$$y^{jl}_m(\hat{\mathbf{p}},\sigma)=\sum_{\nu,\mu}(l\nu\tfrac{1}{2}\mu\,|\,jm)i^lY^l_\nu(\hat{\mathbf{p}})\chi^{1/2}_\mu(\sigma)\ , \tag{7}$$

where Y^l_ν is a spherical harmonic and $\chi^{1/2}_\mu$ is a two-component spinor.

The spin-angle integration in the matrix element of (4) is done by the Wigner-Eckart theorem, for which we use the form

$$\langle jm\,|\,U^{j'}_{m'}\,|\,j''m''\rangle=(-1)^{j-m}\begin{pmatrix} j & j' & j'' \\ -m & m' & m''\end{pmatrix}\times\langle j||\mathbf{U}^{j'}||j'\rangle\ . \tag{8}$$

The reduced matrix element $\langle j||\mathbf{U}^{j'}||j''\rangle$ is a vector in the representation space with equal components. We will evaluate it below in the special case where both the target and the ion are represented by the same independent-particle model. We use the following scalar product:

$$\mathbf{U}^j\cdot\mathbf{V}^j=\sum_m U^{j*}_m V^j_m\ . \tag{9}$$

Applying Eqs. (5) and (8) to matrix elements of (4), we have

$$\langle \mathbf{p}\Psi_f{:}J_fM_f \mid \Psi_0{:}J_0M_0\rangle = \sum_{j,\alpha,m} \phi^j_\alpha(p)\langle \Psi_f{:}J_fM_f \mid a^j_{\alpha m} \mid \Psi_0{:}J_0M_0\rangle \tag{10}$$

$$= \sum_{j,\alpha,m} \phi^j_\alpha(p)(-1)^{J_f-M_f} \begin{pmatrix} J_f & j & J_0 \\ -M_f & m & M_0 \end{pmatrix} \langle \Psi_f||\mathbf{a}^j_\alpha||\Psi_0\rangle \ . \tag{11}$$

The structure factor $G_f(p)$, defined by Eq. (4), is

$$G_f(p)=(2J_0+1)^{-1} \sum_{j,j',\alpha,\beta,m,m'} \phi^j_\alpha(p)\phi^{j'}_\beta(p) \sum_{M_0,M_f} \begin{pmatrix} J_f & j & J_0 \\ -M_f & m & M_0 \end{pmatrix} \begin{pmatrix} J_f & j' & J_0 \\ -M_f & m' & M_0 \end{pmatrix} \langle \Psi_0||(\mathbf{a}^j_\alpha)^\dagger||\Psi_f\rangle\langle \Psi_f||\mathbf{a}^j_\beta||\Psi_0\rangle$$

$$=(2J_0+1)^{-1} \sum_{j,\alpha,\beta} \phi^j_\alpha(p)\phi^j_\beta(p)\langle \Psi_0||(\mathbf{a}^j_\alpha)^\dagger||\Psi_f\rangle\langle \Psi_f||\mathbf{a}^j_\beta||\Psi_0\rangle \ , \tag{12}$$

where the simplification has been effected by using the orthogonality and rearrangement properties of the 3-j symbols.

We now consider only the final states $|\Psi_f{:}J_fM_f\rangle$, which all belong to a symmetry manifold M characterized by J_f and parity and obeying the manifold-closure relation

$$\sum_{f\in M} |\Psi_f{:}J_fM_f\rangle\langle\Psi_f{:}J_fM_f| = 1 \ . \tag{13}$$

The closure property may be used in conjunction with Eq. (12) (in unreduced form) to determine the sum rule for the structure factors belonging to a particular manifold,

$$W_M(p)= \sum_{f\in M} G_f(p)$$

$$=(2J_0+1)^{-1} {\sum_{j,\alpha,\beta}}' \phi^j_\alpha(p)\phi^j_\beta(p)\langle \Psi_0 \mid (\mathbf{a}^j_\alpha)^\dagger\cdot\mathbf{a}^j_\beta \mid \Psi_0\rangle, \tag{14}$$

where the last factor in (14) is just the density matrix for the ground state of the target. The prime over the summation is used to indicate that the sum over orbitals is restricted to those which obey the selection rules implied by (11). We may now define the generalized spectroscopic factor for a particular symmetry manifold by

$$G_f(p)=S_{f,M}(p)W_M(p) \ . \tag{15}$$

It is immediately obvious from definition (14) that the spectroscopic factors obey the sum rule

$$\sum_{f\in M} S_{f,M}(p)=1 \ . \tag{16}$$

In order to obtain a physical understanding of the algebra used for the general case, we evaluate the reduced matrix element for the simplified case of a closed-shell target in which both target and ion are represented by independent-particle determinants of target Hartree-Fock orbitals. We are interested only in the shell characterized by j,α. In this model the probability amplitude that Ψ_f is obtained by annihilating an electron in Ψ_0 is unity:

$$\langle \Psi_f{:}jm \mid a^j_{\alpha m} \mid \Psi_0{:}00\rangle = (-1)^{j-m} \begin{pmatrix} j & j & 0 \\ -m & m & 0 \end{pmatrix}$$

$$\times \langle \Psi_f||\mathbf{a}^j_\alpha||\Psi_0\rangle$$

$$=(2j+1)^{-1/2}\langle \Psi_f||\mathbf{a}^j_\alpha||\Psi_0\rangle = 1 \ .$$

Therefore, in this case

$$\langle \Psi_f||\mathbf{a}^j_\alpha||\Psi_0\rangle = (2j+1)^{1/2} \ . \tag{17}$$

In general, $S_f(p)$ and $W_M(p)$ are calculated by many-body methods such as configuration-interaction or Green's-function methods. However, for many closed-shell targets, nearly 100% of the spectroscopic strength of the many-body wave function Ψ_0 is attributed to the Hartree-Fock (or Dirac-Fock) configuration Φ_0. It is reasonable to make the target Hartree-Fock (or Dirac-Fock) approximation THFA (or TDFA) in which

$$|\Psi_0\rangle = |\Phi_0\rangle \ . \tag{18}$$

This effects an enormous simplification in $G_f(p)$ and $W_M(p)$. Once again, we are interested only in the target shell j,α. For $G_f(p)$ we make the appropriate substitutions in Eq. (12). For a closed shell $J_0=0$. For the single target shell j,α we have $\beta=\alpha$. We express $G_f(p)$ in terms of a spectroscopic factor $S_{f,j\alpha}$, which is 1 in the independent-particle model of the ion, by extracting the factor $(2j+1)^{1/2}$ from each reduced matrix element in accordance with Eq. (17):

$$G_f(p)=[\phi^j_\alpha(p)]^2 \ |\langle \Psi_f||(\mathbf{a}^j_\alpha)^\dagger||\Phi_0\rangle|^2$$

$$=(2j+1)S_{f,j\alpha}[\phi^j_\alpha(p)]^2 \ . \tag{19}$$

The structure factor in the THFA is simply the square of the radial momentum-space orbital multiplied by the electron multiplicity and the spectroscopic factor

$$S_{f,j\alpha}=(2j+1)^{-1} \ |\langle \Psi_f||(\mathbf{a}^j_\alpha)^\dagger||\Phi_0\rangle|^2 \ . \tag{20}$$

In this approximation the spectroscopic factor is independent of p. It is equal to 1 in the approximation that the ion structure is given by a hole in Φ_0. We may consider it as the probability that Ψ_f consists of a hole in Φ_0 with quantum numbers j,α.

For a closed-shell system the ion manifold M is specified by the orbital quantum numbers j,α. The manifold structure factor $W_{j\alpha}(p)$ is obtained by analogy with (15):

$$W_{j\alpha}(p)=[\phi^j_\alpha(p)]^2\langle\Phi_0{:}00\,|\,(\mathbf{a}^j_\alpha)^\dagger\cdot\mathbf{a}^j_\alpha\,|\,\Phi_0{:}00\rangle$$
$$=(2j+1)[\phi^j_\alpha(p)]^2\ . \tag{21}$$

The manifold sum rule (16) in the THFA is

$$\sum_{f\in j\alpha} S_{f,j\alpha}=1\ . \tag{22}$$

Equation (21) gives an experimental definition of the orbital $\phi^j_\alpha(p)$, valid in the case where electron correlation splits the single-particle ion state into fragments f in the manifold $j\alpha$. To the extent that the PWIA and THFA are valid, Eqs. (1), (15), (19), and (21) give

$$[\phi^j_\alpha(p)]^2=(2j+1)^{-1}\sum_{f\in j\alpha}\frac{d^5\sigma_f}{d\hat{\mathbf{k}}_A\,d\hat{\mathbf{k}}_B\,dE_B}\Big/\left[(2\pi)^4\frac{k_Ak_B}{k_0}f_{ee}\right]\ . \tag{23}$$

In practice, differential cross sections for all final states are measured relative to each other. It is not necessary that the PWIA and THFA are valid for absolute cross sections. If $S_{f,j\alpha}$ is independent of momentum, then $\phi^j_\alpha(p)$ may be normalized by (22).

The $(e,2e)$ experiment may be used to provide an experimental measurement of the HF single-particle energy. Using (20), and the algebra leading to (17), we have

$$\epsilon_{j\alpha}=\langle\Phi_0{:}00\,|\,(a^j_{\alpha m})^\dagger H a^j_{\alpha m}\,|\,\Phi_0{:}00\rangle=\sum_{f\in j\alpha,m}\langle\Phi_0{:}00\,|\,(a^j_{\alpha m})^\dagger\,|\,\Psi_f{:}jm\rangle\epsilon_f\langle\Psi_f{:}jm\,|\,a^j_{\alpha m}\,|\,\Phi_0{:}00\rangle=\sum_{f\in j\alpha}S_{f,j\alpha}\epsilon_f\ , \tag{24}$$

where ϵ_f is the experimentally determined separation energy of the state f.

We have carried out relativistic configuration-interaction calculations for the xenon ground state $|\Psi_0\rangle$ (see Sec. IV for details) and find that $|\langle\Phi_0|\Psi_0\rangle|^2\gtrsim 0.95$, where $|\Phi_0\rangle$ is the Dirac-Fock configuration for the xenon ground state. Consequently, those terms of Eq. (12), involving ejection of an electron from a target DF orbital, will dominate these matrix elements, and so cause the generalized spectroscopic factors to be almost independent of p. Therefore, for detailed comparison with the experiment we use primarily the TDFA (or THFA) in conjunction with the DWIA.

Expression (19) for the structure factor $G_f(p)$ is replaced by

$$G_f(p)=S_{f,j\alpha}\sum_m|\langle\chi^{(-)}(\mathbf{k}_A)\chi^{(-)}(\mathbf{k}_B)\,|\,\phi^j_{\alpha m}\chi^{(+)}(\mathbf{k}_0)\rangle|^2\ , \tag{25}$$

where $\chi^{(\pm)}(\mathbf{k})$ are elastic-scattering wave functions for electrons in the appropriate equivalent local static exchange potentials. Spin-orbit coupling is omitted from these potentials.

For ϕ^j_α we use a target Hartree-Fock or Dirac-Fock orbital. Only the large component is used in the distorted-wave DF calculation. We have tested the validity of this approximation for xenon by computing PWIA cross sections using, alternatively, the large component and both components. The error involved is less than 1%.

III. EXPERIMENTAL METHOD

Noncoplanar symmetric geometry was used in the present work. The electron-coincidence spectrometer and the techniques used have been described previously,[3,4] and only a brief outline will be given here. A schematic diagram of the instrument and associated electronics is given in Fig. 1. Details of the construction, as well as the computer-controlled operation and data analysis of this instrument, are given in Refs. 3 and 4. One major change has been to replace the deceleration lens by a five-element lens similar to that described by Kevan,[9] which allows adjustment in the angle of acceptance. In the present work it was fixed at $\Delta\phi\approx\Delta\phi\approx 1°$ full width.

Electrons from a differentially pumped electron gun pass through a gas target chamber, the xenon gas being admitted to the collision region through a capillary tube. The two outgoing electrons are detected by twin electron spectrometers which have position-sensitive microchannel plate detectors mounted at their exits in order to allow a range of energies to be measured simultaneously. Binding-energy spectra at a series of relative azimuthal angles ϕ were obtained in a binning mode in which the spectrum was windowed across the microchannel plates so that each part of the spectrum was collected for an equal time on each part of the channel plates. Momentum distributions were obtained from sequentially obtained angular correlated binding-energy spectra in order to maintain relative normalizations. In any run the binding-energy spectra at the different relative azimuthal angles were scanned repeatedly over the whole angular range.

The operating conditions at 1000 eV were $E_0=1000$ eV + separation energy, $E_A=E_B=500$ eV, $\theta=45°$, and $\phi=\pi-\phi_A-\phi_B$ was varied over the range 0°–35°. Momentum resolution was $\lesssim 0.06a_0^{-1}$, while the energy resolution was 1.2 eV full width at half maximum (FWHM). The experimental energy-resolution function was obtained by accurate measurements of the He$(e,2e)$He$^+$ ground-state transition. Data were also taken at 1200 eV, with $E_0=1200$ eV + separation energy, $E_A=E_B=600$ eV, $\theta_A=\theta_B=45.75°\pm 0.25°$, angular resolution $\Delta\theta=\Delta\phi\sim 1°$ FWHM, and an energy resolution of 1.5 eV FWHM.

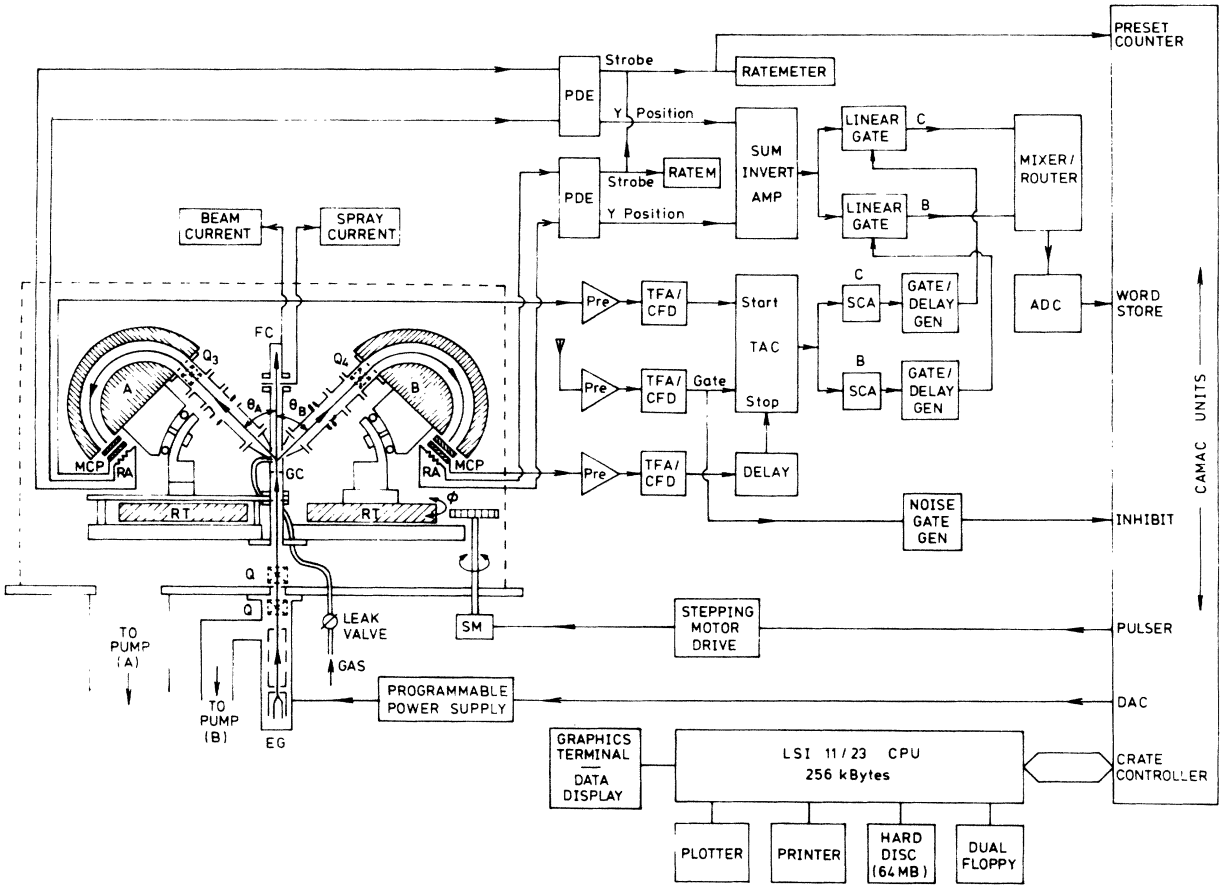

FIG. 1. Schematic diagram of the noncoplanar symmetric coincidence spectrometer and associated electronics. MCP, microchannel plates with resistive anodes (RA); RT, rotating turntable on which hemispherical analyzer B is mounted; SM, stepping motor for setting the out-of-plane azimuthal angle; Q, quadrupole deflectors; EG, differentially pumped electron gun; PDE, position-determining electronics; TFA/CFD, timing-filter amplifier and constant-fraction discriminator.

IV. RESULTS AND DISCUSSION

A. Structure calculations and spectroscopic factors

1. The $5s^{-1}$ transition

The extreme complexity of the inner-valence separation-energy spectrum can be seen in Fig. 2, which shows the measured inner-valence separation-energy spectrum at 1000 eV and $\phi=0°$. The spectroscopic factors for the $5s^{-1}$ transitions obtained at this angle ($p\approx 0.1$ a.u.), and at $\phi=8°$ ($p\approx 0.6$ a.u.), are shown in Table I. The spectroscopic factors have been normalized to unity using the sum rule (22). Table II reports the $5s^{-1}$ spectroscopic factors obtained at 1200 eV over a range of azimuthal angles, i.e., electron momenta p. The 1000- and 1200-eV data are in agreement within experimental error, as are the spectroscopic factors at the different values of recoil momenta. The data show that the spectroscopic factor for the "main" $5s^{-1}$ transition leading to the $5s\,5p^6\ {}^2S_{\frac{1}{2}}^+$

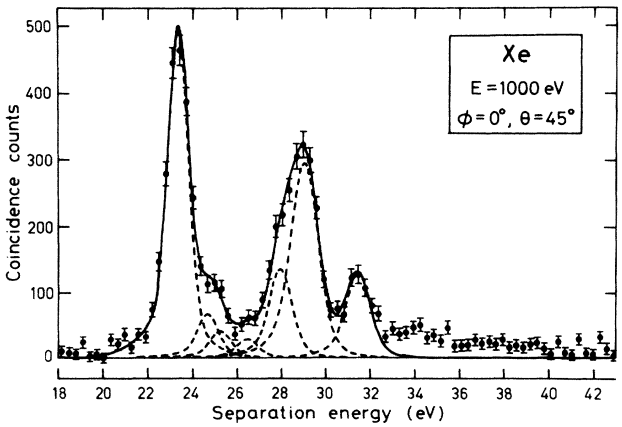

FIG. 2. The 1000-eV noncoplanar symmetric separation-energy spectrum of xenon at $\phi=0°$ and $\theta=45°$ over the (22—45)-eV region. The solid curve shows the least-squares fit to the data with peaks at 23.4, 24.7, 25.3, 26.5, 28.0, 29.1, and 31.5 eV.

TABLE I. The Xe $5s^{-1}$ spectroscopic factors normalized to unity at $E=1000$ eV and $\theta=45°$ for transitions with the indicated separation energies. The dominant configuration of the corresponding ion eigenstate is also shown. The errors in the last significant figure for spectroscopic factors at a given azimuthal angle are given in the parentheses.

ϵ (eV)	Dominant configuration	$\phi=0°$ $p\approx0.1$ a.u.	$\phi=8°$ $p\approx0.6$ a.u.
23.4	$5s\,5p^6\ ^2S$	0.36(1)	0.34(2)
24.7	$5s^2 5p^4(^3P)6s\ ^4P$	0.04(1)	0.02(2)
25.3	$5s^2 5p^4(^3P)5d\ ^4P$	0.03(1)	0.05(2)
26.5		0.02(1)	0.01(2)
28.0	$5s^2 5p^4(^1D)5d\ ^2P$ $5s^2 5p^4(^1S)6s\ ^2S$	0.11(1)	0.12(2)
29.1	$5s^2 5p^4(^1D)5d\ ^2S$ $5s^2 5p^4(^3D)6d\ ^4P$ $5s^2 5p^4(^3P)6d\ ^4P$	0.24(1)	0.22(2)
31.5	$5s^2 5p^4(^1D)6d\ ^2P$ $5s^2 5p^4(^1D)6d\ ^2S$	0.10(1)	0.10(2)
$\gtrsim 33.4$ <45	$Xe^{2+}+e$	0.11(1)	0.14(2)

ion state at 23.4 eV is only 0.37 ± 0.01, with approximately 12% of the $5s^{-1}$ strength lying in the continuum.

The relative spectroscopic factors for the two main transitions are plotted in Fig. 3 as a function of the recoil momentum for both the 1200-eV data (circles) and 1000-eV data (triangles). The spectroscopic factors are independent of momentum and incident-electron energy.

Exact comparison of the present EMS data with the relative intensities of the main $5s^{-1}$ and satellite lines in Xe photoelectron spectra is not possible. There are several reasons for this.[10] The first is that the photoelectron-spectroscopy (PES) data are measured at much higher ion-recoil momenta, $p\approx3$ a.u. for $h\nu\approx130$ eV and $p\approx10$ a.u. for $h\nu\approx1487$ eV. Our data (see Sec. IV B) show that even for 500-eV outgoing electrons the distortion from plane waves is significant for $p\gtrsim1.5$ a.u. The high-momentum component of the electron wave function is dominated by the wave function close to the nucleus, where the distorting potential is greatest. Thus in PES, as one increases the photon energy one selects electrons of higher momentum from, on the average, an increasingly large distorting potential, and it is doubtful if the electron waves can ever accurately be described by plane waves. This makes it difficult to extract meaningful spectroscopic factors. Another reason is that as the momentum component increases, the presence of very small electron-correlation effects in the target wave function may become more important.[4] In addition, much of the PES data, such as that of Gelius[11] and Spears *et al.*,[12] were recorded at 90° rather than the "magic" angle, which makes it difficult to interpret the reported relative intensities since the asymmetry parameter may be state and energy dependent. Above the double-ionization threshold or in any region where the peaks are not well separated, PES is beset by background-subtraction problems,[13] which make the interpretation of PES data in those regions extremely unreliable.

We have carried out relativistic configuration-interaction calculations of the target atom and residual ion states in order to identify the causes of the complex structure associated with the $5s^{-1}$ manifold. The calculations were also undertaken to determine whether initial- and final-state configuration interactions (CI's) have any influence upon the $5p_{3/2}^{-1}$:$5p_{1/2}^{-1}$ cross-section ratio. That relativistic effects need to be incorporated for the determination of the spectroscopic factors for $5s^{-1}$ manifold (as well as the $5p^{-1}$ states) is most easily seen by comparing results of a ground-state multiconfiguration Hartree-Fock[14] (MCHF) calculation and the equivalent multiconfiguration Dirac-Fock optimal level (MCDF-OL) calculation,[15] including the $5s\,5p^6$ and $5s^2 5p^4 5d$ configurations. The dimensionality of the MCHF calculation was two, while that for the relativistic calculation was six. The $5s\,5p^6$ configuration probability (given in Table III) for the lowest $J^\pi=\frac{1}{2}^+$ state is about 0.1 smaller for the MCDF calculation than for the equivalent MCHF calculation and in better agreement with the $(e,2e)$ spectroscopic factor. We also note that three of the other $J^\pi=\frac{1}{2}^+$ states have configuration probabilities greater than 0.01, demonstrating the breakdown of LS coupling in the Xe II spectrum. Indeed, some semiphenomenological calculations by Hansen and Persson[16] have demonstrated that the $J^\pi=\frac{1}{2}^+$ $(5s^{-1})$ manifold is extremely complex and cannot be easily described by any coupling scheme. Hansen and Persson also derived $5s\,5p^6$ configuration probabilities from their analysis. These are detailed in Table IV.

The scheme used for the CI calculation uses orbitals

TABLE II. The Xe $5s^{-1}$ pole strengths at $E=1200$ eV and $\theta=45.7°$ for transitions with the indicated separation energies as a function of the out-of-plane azimuthal angle (i.e., recoil momentum p). The number in parentheses gives the error in the last significant figure.

ϵ (eV)	Dominant configuration	$\phi=0°$ $p\approx 0.3$ a.u.	$=3°$ ≈ 0.4 a.u.	$=5°$ ≈ 0.5 a.u.	$=6°$ ≈ 0.6 a.u.	$=8.5°$ ≈ 0.75 a.u.	$=11.5°$ ≈ 1.0 a.u.	$=15°$ ≈ 1.2 a.u.	$=18°$ ≈ 1.5 a.u.
23.4	$5s5p^6\ ^2S$	0.38(2)	0.37(3)	0.38(3)	0.39(3)	0.37(3)	0.32(4)	0.37(4)	0.37(4)
24.7	$5s^25p^4(^3P)6s\ ^4P$	0.03(2)	0.03(3)	0.05(3)	0.05(3)	0.02(3)	0.03(4)	0.01(4)	0.01(4)
25.3	$5s^25p^4(^3P)5d\ ^4P$	0.04(2)	0.02(3)	0.03(3)	0.02(3)	0.08(3)	0.04(4)	0.02(4)	0.03(4)
28.0	$5s^25p^4(^1D)5d\ ^2P$ $5s^25p^4(^1S)6s\ ^2S$	0.11(2)	0.13(3)	0.12(3)	0.09(3)	0.10(3)	0.19(4)	0.15(4)	0.14(4)
29.1	$5s^25p^4(^1D)5d\ ^2S$ $5s^25p^4(^3D)6d\ ^4P$ $5s^25p^4(^3P)6d\ ^4P$	0.25(2)	0.24(3)	0.23(3)	0.25(3)	0.24(3)	0.22(4)	0.22(4)	0.23(4)
31.5	$5s^25p^4(^1D)6d\ ^2P$ $5s^25p^4(^1D)6d\ ^4S$	0.08(2)	0.09(3)	0.09(3)	0.08(3)	0.08(3)	0.08(4)	0.09(4)	0.09(4)
33.4–40	$Xe^{2+}+e$	0.11(2)	0.12(3)	0.12(3)	0.12(3)	0.11(3)	0.12(4)	0.14(4)	0.13(4)

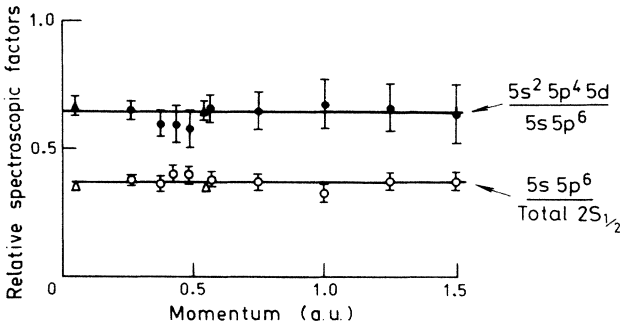

FIG. 3. Relative spectroscopic factors in the $5s^{-1}$ manifold plotted as a function of the ion-recoil momentum. The open and solid circles are from the 1200-eV data and the open and solid triangles from the 1000-eV data.

generated by the Grant *et al.* MCDF (Ref. 15) program as input for a general CI program using the m-scheme approach developed by Mitroy *et al.*[17,18] The $5s$ and $5p$ orbitals (as well as the $1s$-$4d$ inert core) were determined by a calculation of the Xe I ground state. In addition $\overline{6s}$, $\overline{6p}$, and $\overline{5d}$ orbitals were generated with approximately the same radial expectation value, $\langle r\rangle$, as the $5s$ and $5p$ orbitals by calculations on multiply ionized xenon configurations. The purpose of these orbitals is to allow for correlations and relaxations of the $5s$ and $5p$ orbitals, and additionally for the $\overline{5d}$ orbital to allow for interactions between the bound $\frac{1}{2}^+$ states and the $5s^25p^4\epsilon d$ continuum. The $5d$, $6s$, $6p$, $7s$, and $6d$ orbitals were generated from frozen-core (including the $5s$ and $5p$ orbitals) extended-average-level (EAL) calculations of the $5s^25p^4nl$ manifolds. All these orbitals were Schmidt-orthogonalized in the order they were mentioned in the text above.

First, a rather simple calculation was performed for the $5s^{-1}$ manifold, including only the $5s5p^6$, $5s^25p^4(\overline{5d}+\overline{6s}+5s+6s+6d+7s)$ configurations. The $5s5p^6$ configuration probabilities and excitation energies for all states are given in Table IV. The energy separation between the Xe II ground state and the Xe I DF ground state was slightly too small. This was also found to be the

TABLE III. A comparison of $5s5p^6$ configuration probabilities for nonrelativistic MCHF and relativistic MCDF-OL calculations incorporating the $5s5p^6$ and $5s^25p^4\overline{5d}$ configurations. Only two configurations [the $5s5p^6$ and $5s^25p^4(^1D^e)\overline{5d}\ ^2S^e$] were included in the nonrelativistic MCHF calculation. Due to the use of jj coupling in the MCDF-OL calculation, the dimensionality was six since there are five $5s^25p^4\overline{5d}$ configurations with $J^\pi=\frac{1}{2}^+$.

State no.	MCHF	MCDF-OL
1	0.620	0.536
2		<0.001
3		<0.001
4		0.020
5		0.028
6	0.380	0.416

TABLE IV. Calculated $5s5p^6$ configuration probabilities and separation energies (in eV) for the low-lying $J^\pi=\frac{1}{2}^+$ states. Columns labeled calculations 1 and 2 come from the small and large-basis CI calculations described in the text. Spectroscopic factors computed using Eq. (15) are also reported for our large-basis calculation. It is not possible to give the eigenstates a designation in terms of a single configuration since most of the states are not dominated by a single configuration.

	Calculation 1		Calculation 2			Ref. 16	
State	ϵ_f	$5s5p^6$ (%)	ϵ_f	$5s5p^6$ (%)	S_f $(p=0.1)$	ϵ_f	$5s5p^6$ (%)
1	22.77	0.527	24.52	0.513	0.481	23.40	0.455
2	23.99	0.001	25.67	0.001	0.001	24.14	0.001
3	24.92	0.020	26.12	0.018	0.019	24.67	0.030
4	25.16	0.003	26.72	0.001	0.001	25.06	0.001
5	25.58	0.017	27.01	0.017	0.016	25.27	0.036
6	25.98	0.001	27.13	0.005	0.005	25.39	0.005
7	28.90	0.036	29.12	0.021	0.024	27.88	0.041
8	29.19	0.001	30.31	0.006	0.006	28.16	0.015
9	29.46	0.001	30.71	0.003	0.003	28.88	0.214
10	30.01	0.001	31.21	0.001	0.001	29.06	0.016
11	30.19	0.002	31.22	0.005	0.005	29.33	0.122
12	30.55	0.003	31.62	0.002	0.002	29.60	0.004
13	30.67	0.171	31.77	0.176	0.180	29.85	0.000
14	30.82	0.0	32.00	0.0	0.0	30.14	0.000
15	32.31	0.013	33.51	0.011	0.012	31.43	0.031
16	32.71	0.134	33.86	0.116	0.120	31.53	0.002
17	34.13	0.003	34.67	0.007	0.006	31.59	0.027

case in a similar calculation of the argon $(e,2e)$ spectrum.[8] As expected, the pole strength for the primary transition is not significantly different from that obtained by the MCDF-OL calculation. The results for all the satellite states show qualitative agreement with most of the features of the $(e,2e)$ spectrum, although there are some distinctions. In particular, the energy spacings between the levels are too large, but this is to be expected since the $5s$ and $5p$ orbitals are identical for all states. Another defect is that the predicted strengths of those states which primarily result from intermediate coupling are underestimated.

In order to improve our model, we have used this configuration set as a reference set to generate a more extensive CI basis including those configurations which could be created by single and double excitations into the $\overline{6s}$ and $\overline{6p}$ orbitals. While it would have been desirable to have included the excitations into the $\overline{5d}$ orbitals, the resulting dimensionality of the basis [$\approx$4000 $\frac{1}{2}^+$ states comprising $\approx$26 000 Slater determinants (SD's)] was three times larger than the equivalent nonrelativistic calculation and was marginally too large for our available computing resources. There is a slight improvement in the results (Table IV), with the spacings between the levels being reduced and the $5s5p^6$ configuration probabilities of the satellite states being marginally increased.

When a large-basis CI calculation for the target is performed and the resulting wave function used in the calculation of the spectroscopic factors, improved agreement with experiment is achieved. Although the spectroscopic factors are then, in principle, a function of the recoil momentum p, the calculation showed that the differences between the spectroscopic factors at $p=0.1$ and 0.5 a.u. were insignificant. Since single and double excitations from the $5s$ and $5p$ orbitals into the $\overline{5d}$ orbital were allowed (in the target wave function) it was also possible to estimate whether the population of $\frac{3}{2}^+$ and $\frac{5}{2}^+$ ion states (through d-electron knockout) could be hidden by the complexity of the spectrum. We found that the sum total of the strength of the $\frac{3}{2}^+$ and $\frac{5}{2}^+$ manifolds was less than 1% of the strength of the $\frac{1}{2}^+$ manifold for $p<0.8$ a.u., and was insignificant at $p=0.2$ and 0.5 a.u. when compared with the strength of the $\frac{1}{2}^+$ manifold.

Since the TDFA is valid to a high degree of accuracy, we can use Eq. (24) to calculate the $5s$-orbital energy despite the large splitting observed in the $5s^{-1}$ manifold. The observed orbital energy is 27.6 ± 0.3 eV, in agreement with the calculated DF value of 27.49 eV, and can be compared with the HF value of 25.70 eV.

2. *The $5p^{-1}$ transitions*

The $5p_{3/2}^{-1}$ and $5p_{1/2}^{-1}$ transitions at separation energies of 12.13 and 13.43 eV, respectively, were investigated in detail at 1200 eV and the angular correlations reported in Ref. 7. The $5p_{3/2}^{-1}$ and $5p_{1/2}^{-1}$ momentum densities and branching ratios could not be described by nonrelativistic wave functions, but they were found to be in excellent agreement with those given by Dirac-Fock wave functions.[7]

Since the $5p^{-1}$ angular correlations are quite distinct from the $5s^{-1}$ angular correlations (see Figs. 4 and 5), it is easy to separate $5p^{-1}$ satellite structure from the $5s^{-1}$ structure. From binding-energy spectra taken at $\phi=0°$, where the $5s^{-1}$ cross section is a maximum and the $5p^{-1}$ is at a minimum, and at $\phi=6°$–$8°$, where the $5p^{-1}$ cross section is maximum and the $5s^{-1}$ cross section has dropped away to less than one-third of its maximum

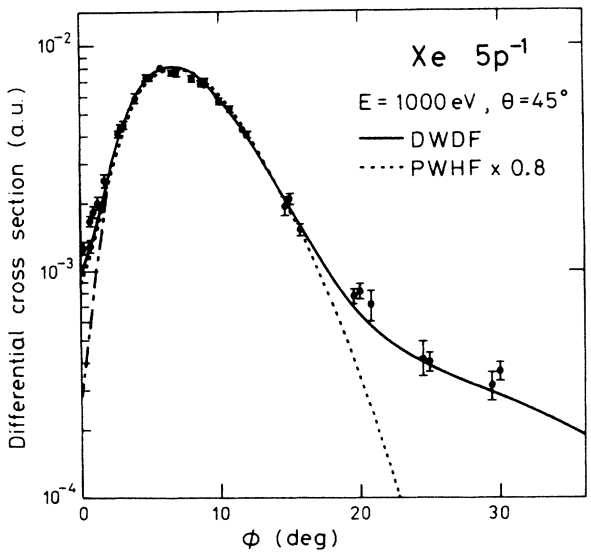

FIG. 4. The experimental angular correlation at 1000 eV for the xenon total $5p^{-1}$ ground-state transition normalized to the DWIA—Dirac-Fock cross section at $\phi = 5°$ (solid curve). The DWIA—Hartree-Fock cross section is indistinguishable from the DF cross section, whereas the PWIA-DF cross section is indicated by the dashed curve. The dashed-dotted curve at small angles indicates the DWIA and PWIA cross sections if no allowance is made for the finite angular resolutions of the spectrometers.

value, we are able to establish an upper bound of 0.015 ± 0.005 for the summed spectroscopic strength for $5p^{-1}$ transitions in the separation energy range 23.4—45 eV. Significant additional $5p^{-1}$ strength with separation energy greater than 45 eV is highly unlikely. This implies that the primary transitions to the $5p^{-1}$ states must have spectroscopic strengths of at least 0.98. A large-basis CI calculation was undertaken in order to provide a theoretical verification.

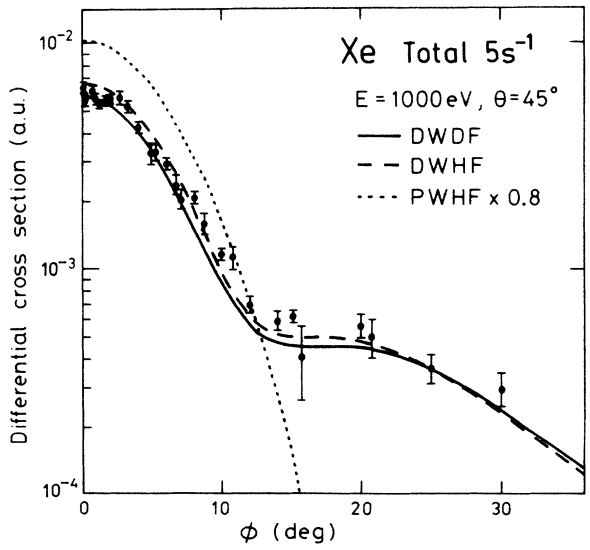

FIG. 5. Angular correlations at 1000 eV for the total $5s^{-1}$ cross section compared to the DWIA and PWIA using Dirac-Fock and Hartree-Fock target wave functions. The $5p^{-1}$ normalization (Fig. 4) serves to normalize the $5s^{-1}$ data since relative cross sections are measured.

For the calculation of the $5p_{1/2}^{-1}$ and $5p_{3/2}^{-1}$ states, the $5s^2 5p^5$, $5s^2 5p^4 6p$, and $5s^2 5p^4 \overline{6p}$ manifolds were chosen as the reference configuration set, and all possible configurations that could be formed from single and double excitation from the reference set into the $\overline{6s}$, $\overline{6p}$, $\overline{5d}$, and $6s$ orbitals were used to construct the CI basis. Both the $5p_{1/2}^{-1}$ and $5p_{3/2}^{-1}$ states were well described by the one-hole configurations, the calculated configuration probabilities being 0.927 and 0.931, respectively. The calculated energy splitting of 0.048 08 a.u. for the doublet compares well with the empirical value of 0.0478 a.u., and is much better than the value of 0.052 75 obtained by using Koopmans's theorem. The configuration probabilities obtained from our calculations for the $5p_{3/2}^{-1}$ and $5p_{1/2}^{-1}$ ion states seem to indicate that it might be possible that up to 7% of the $5p^{-1}$ strength could possibly interfere with the $5s^{-1}$ manifold and distort the $5s^{-1}$ experimental spectroscopic factors at higher q values. However, this inconsistent treatment of the target and ion wave functions (a single configuration for the target, many configurations for the ion states) leads to spectroscopic factors which are systematically too low.[8] More accurate values for the spectroscopic factors were computed using a large-basis CI wave function (all single and double excitations into the $\overline{5d}$, $\overline{6s}$, $\overline{6p}$, $6s$, and $6p$ orbitals) for the Xe I ground-state wave function and evaluating Eq. (12). The resulting spectroscopic factors at $p = 0.5$ a.u. are 0.980 and 0.983, respectively, for the $5p_{3/2}^{-1}$ and $5p_{1/2}^{-1}$ transitions. Furthermore, the $5p_{3/2}^{-1}$ and $5p_{1/2}^{-1}$ cross-section ratios were found to be quite insensitive to initial- and final-state configuration interactions, being practically identical to the DF ratio depicted in Fig. 6 for all q values shown.

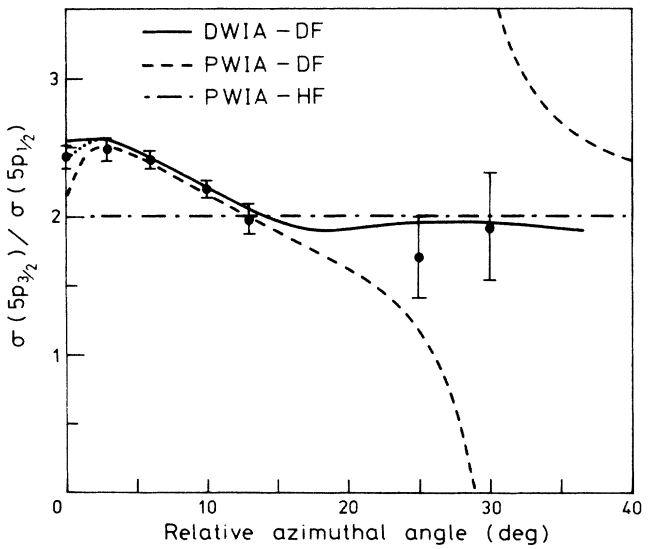

FIG. 6. The $5p_{3/2}^{-1}$:$5p_{1/2}^{-1}$ branching ratios at 1000 eV plotted as a function of the out-of-plane azimuthal angle. The solid curve is the DWIA-DF result including the effects of finite angular resolution. The dotted curve at small angles shows the DWIA-DF result if no allowance is made for finite angular resolution. The PWIA-DF ratio has a singularity at about 30° because the PWIA for the $5p_{1/2}^{-1}$ and $5p_{3/2}^{-1}$ transitions has unphysical zeros at different momenta, corresponding to the zeros of the momentum-space orbitals.

B. The noncoplanar symmetric (e,2e) cross section

The 1000-eV noncoplanar symmetric $(e,2e)$ cross sections have been measured for the $5p^{-1}$ transition and for the range of the states in the $5s^{-1}$ manifold (see Table II). All cross sections are measured relative to each other, so that it is necessary to normalize the experiment at one point for comparison with theory. We have chosen this point to be $\phi=5°$ for the combined $5p_{3/2}^{-1}$ (12.13 eV) and $5p_{1/2}^{-1}$ (13.43 eV) transition. The results are shown in Figs. 4 and 5 for the $5p^{-1}$ and $5s^{-1}$ transitions, respectively. A logarithmic plot has been chosen to exhibit the small cross-section region. Three calculations are compared with the data: (1) DWDF—the distorted-wave impulse approximation (DWIA) using the Dirac-Fock approximation for the xenon ground state; (2) DWHF—the DWIA using the Hartree-Fock approximation for the target; and (3) PWHF—the plane-wave impulse approximation (PWIA) with the Hartree-Fock approximation for the target. In Fig. 4 the DWHF results are not shown since they are essentially indistinguishable from the sum of the $5p_{3/2}^{-1}$ and $5p_{1/2}^{-1}$ DWDF cross sections. We have also included the effects of the finite angular resolution of the electron detectors in our calculations by integrating the cross sections over a small range of $\Delta\theta$ and $\Delta\phi$ representative of the experimental resolution. For the $5s^{-1}$ cross section (Fig. 5), the angular resolution effects were negligible. However, for the $5p^{-1}$ cross section (Fig. 4), the finite-angular-resolution effects were significant for out-of-plane azimuthal angles $\phi \lesssim 2°$. The DWDF, DWHF, and PWHF cross sections without allowance for finite acceptance angles are shown by the dashed-dotted curve in Fig. 4, which underestimates the measured cross section at small angles ϕ.

The DWIA gives an excellent description of all of the data. The PWIA gives a good description of the $5p^{-1}$ cross section over the range 0°–16°. This is the most important part of the cross section in terms of momentum spectroscopy, since it corresponds to ion-recoil momenta p of less than or approximately 1.5 a.u. This range of momentum covers the chemically interesting region of the momentum-space wave function. The PWIA cross section is approximately 20% larger than the DWIA cross section in this region (cf. the normalization factor of 0.8).

Figure 5 shows the measured angular correlation for the $5s^{-1}$ manifold compared with the calculated cross sections. The solid line shows the DWDF cross sections normalized to the $5p^{-1}$ cross section at 5°. The dashed line shows the DWHF cross section, which differs significantly from the DWDF cross section, but both are in approximately equal agreement with the data. The PWIA seriously overestimates the $5s^{-1}$ cross section for $\phi \lesssim 12°$, and underestimates it in the higher angular range. The shape in the region $\phi \lesssim 10°$ is nevertheless well described by the PWIA. This again is the low-momentum region, where the momentum density of the struck electron is largest.

Not only does the DWIA describe the shapes of the angular correlations within experimental error, but it confirms the spectroscopic analysis of the $5p^{-1}$ and $5s^{-1}$ manifolds. In Figs. 4 and 5 the total spectroscopic strengths for the $5p^{-1}$ and $5s^{-1}$ transitions are taken to be unity. The success of the DWIA at 1000 eV in the case of xenon repeats its success at the same energy for the lighter noble-gas atom argon.[3]

In the above analysis we have assumed the THFA or the TDFA. If target correlations are permitted, then the matrix element becomes a linear combination of the different terms depending on the particular orbital from which an electron has been ejected, and the spectroscopic factor depends on p. We have carried out calculations of the PWIA structure factors (using the large-basis CI wave functions) to determine the $5s^{-1}$ and $5p^{-1}$ spectroscopic factors as a function of p. The spectroscopic factors were found to be independent of p to well within experimental accuracy (Table II and Fig. 3).

C. The $5p_{3/2}^{-1}$:$5p_{1/2}^{-1}$ branching ratios

The 1200-eV $5p_{3/2}^{-1}$:$5p_{1/2}^{-1}$ branching ratios were reported by us in an earlier publication.[7] They were in agreement with the ratios given by the DF wave functions and in disagreement with the constant statistical weight ratio of 2, which is predicted by the HF theory. The 1200-eV data were analyzed using the PWIA.

In Fig. 6 we show the ratio measurements obtained at 1000 eV compared with the DWIA and PWIA results using $5p_{3/2}$ and $5p_{1/2}$ DF wave functions and the HF value of 2. The effects of finite angular resolution have been included in the DWIA calculation, where again the only significant effects are for $\phi \lesssim 2°$. The dotted curve at small ϕ indicates the DWIA results without any allowance for finite angular resolution, while the dashed curve gives the PWIA result.

The data are in excellent agreement with the DWDF results. As expected, the PWIA cross-section ratios differ significantly from the DWIA results for large angles ϕ ($\gtrsim 17°$), where the cross section is very small. The data once again demonstrate the inadequacy of the HF wave functions for xenon. The calculated ratios shown in Fig. 6 are obtained using the THFA or TDFA. However, as discussed in Sec. IV A, we checked the validity of these approximations by carrying out calculations using the large-basis CI wave functions for the initial and final states. These calculations showed that the $5p_{3/2}^{-1}$ and $5p_{1/2}^{-1}$ cross-section ratios are quite insensitive to initial- and final-state electron-correlation effects.

V. SUMMARY

We have compared accurate 1000-eV noncoplanar symmetric $(e,2e)$ cross sections at $\theta=45°$ for the $5p^{-1}$ and $5s^{-1}$ manifolds of xenon with the factorized distorted-wave half-off-shell impulse approximation using either plane waves (PWIA) or full partial-wave-expanded static exchange wave functions for the continuum electron waves (DWIA). The DWIA describes the whole experiment within experimental error. Furthermore, it throws light on the determination of spectroscopic factors without recourse to detailed theory. Spectroscopic factors for the $5s^{-1}$ manifold are correctly determined by comparing cross sections for the states within the manifold at

the angle ϕ for the maximum cross section.

The PWIA gives a good description of the shapes of the angular correlations at small angles ϕ ($\lesssim 15°$), where the cross sections are large. This is the most important part of the cross section in terms of momentum spectroscopy, since it corresponds to ion-recoil momenta of less than or approximately 1.5 a.u. This range of momentum covers the chemically interesting region of the momentum-space wave function. The PWIA can readily be used to identify the manifold to which a particular transition belongs, and hence to calculate relative spectroscopic factors within a manifold. It does, however, overestimate the cross section for the inner-valence transitions relative to the outer-valence (ground-state) cross section. The DWIA obtains the correct cross-section ratios for the different manifolds.

The $5p^{-1}$ ground-state transition is shown to be an almost pure independent-particle transition with a spectroscopic factor greater than or equal to 0.98. This is verified by detailed MCDF-OL calculation of the atom and ion ground states. The $5p_{3/2}^{-1}$:$5p_{1/2}^{-1}$ branching ratio cannot be explained using HF wave functions since it changes from almost 2.5 at small ϕ to a little less than 2 at larger ϕ. The branching ratios are, however, in excellent agreement with the values given by the $5p_{3/2}$ and $5p_{1/2}$ DF wave functions. This is in agreement with our earlier measurements[7] at 1200 eV.

The $5s^{-1}$ manifold, on the other hand, is severely split, with the strength of the "main" transition at 23.4 eV being only 0.37 ± 0.01. The spectroscopic strengths for various transitions, including the continuum above the double-ionization threshold at both 1000 and 1200 eV, are, within experimental error, independent of energy and ion-recoil momentum, thus verifying the analysis of the $5s^{-1}$ manifold. MCDF-OL calculations are only in qualitative agreement with the data, somewhat underestimating the severity of the splitting of the $5s^{-1}$ manifold.

[1]I. E. McCarthy and E. Weigold, Phys. Rep. **27c**, 275 (1976); E. Weigold and I. E. McCarthy, Adv. At. Mol. Phys. **14**, 127 (1978).
[2]A. J. Dixon, I. E. McCarthy, C. J. Noble, and E. Weigold, Phys. Rev. A **17**, 597 (1978).
[3]I. E. McCarthy and E. Weigold, Phys. Rev. A **31**, 160 (1985).
[4]J. P. D. Cook, I. E. McCarthy, A. T. Stelbovics, and E. Weigold, J. Phys. B **17**, 2339 (1984).
[5]I. Fuss, J. Mitroy, and B. M. Spicer, J. Phys. B **15**, 3321 (1982).
[6]A. Ugbabe, E. Weigold, and I. E. McCarthy, Phys. Rev. A **11**, 576 (1975).
[7]J. P. D. Cook, J. Mitroy, and E. Weigold, Phys. Rev. Lett. **52**, 1116 (1984).
[8]J. Mitroy, K. Amos, and I. Morrison, J. Phys. B **17**, 1659 (1984).
[9]S. D. Kevan, Rev. Sci. Instrum. **54**, 1441 (1983).
[10]E. Weigold, Comments At. Mol. Phys. **15**, 223 (1984).
[11]U. Gelius, J. Electron Spectrosc. **5**, 984 (1984).
[12]D. Spears, E. J. Fishbeck, and T. A. Carlson, Phys. Rev. A **9**, 1603 (1974).
[13]J. Mitroy, I. E. McCarthy, and E. Weigold, J. Phys. B **18**, L91 (1985).
[14]C. Froese-Fischer, Comput. Phys. Commun. **14**, 145 (1978).
[15]I. P. Grant, B. J. McKenzie, P. H. Norrington, D. F. Mayers, and N. C. Pyper, Comput. Phys. Commun. **21**, 207 (1980).
[16]J. E. Hansen and W. Persson, Phys. Rev. A **18**, 1459 (1978).
[17]J. Mitroy and I. Morrison, J. Phys. B **17**, 4449 (1984).
[18]J. Mitroy, K. Amos, and I. Morrison, J. Phys. B **12**, 1081 (1979).